

A region-growing approach for automatic outcrop fracture extraction from a three-dimensional point cloud

Xin Wang^a, Lejun Zou^a, Xiaohua Shen^a, Yupeng Ren^a, Yi Qin^a

^a*Department of Earth Sciences, Zhejiang University Yuquan Campus, 38 Zheda Road, Hangzhou 310027, China*

Abstract

Conventional manual surveys of rock mass fractures usually require large amounts of time and labor; yet, they provide a relatively small set of data that cannot be considered representative of the study region. Terrestrial laser scanners are increasingly used for fracture surveys because they can efficiently acquire large area, high-resolution, three-dimensional (3D) point clouds from outcrops. However, extracting fractures and other planar surfaces from 3D outcrop point clouds is still a challenging task. No method has been reported that can be used to automatically extract the full extent of every individual fracture from a 3D outcrop point cloud. In this study, we propose a method using a region-growing approach to address this problem; the method also estimates the orientation of each fracture. In this method, criteria based on the local surface normal and curvature of the point cloud are used to initiate and control the growth of the fracture region. In tests using outcrop point cloud data, the proposed method identified and extracted the full extent of individual fractures with high accuracy. Compared with manually acquired

Email addresses: ericrussell@zju.edu.cn (Xin Wang), shenxh@zju.edu.cn (Xiaohua Shen)

field survey data, our method obtained better-quality fracture data, thereby demonstrating the high potential utility of the proposed method.

Keywords:

Outcrop fracture surveys; Terrestrial laser scanner; LiDAR; Point cloud; Automatic extraction; Region-growing-based algorithm

1. Introduction

The manual surveying of fractures and other planar rock mass surfaces is one of the most fundamental but time-consuming activities performed by field geologists. The surveyed fracture data usually comprise the fracture location, orientation, and surface roughness, which can support models and/or hypotheses in various applications (e.g., structural and geomechanical analysis, flow modeling, reservoir characterization, and engineering rock mass classification). These surveys are conventionally performed in situ with standard fieldwork instruments, such as a handheld compass, clinometer, and possibly a digital camera to record the fracture locations. However, the development of remote sensors (e.g., LiDAR-based scanners) and their availability as research equipment have prompted geoscientists to develop new methods that improve the analysis, avoid access problems, reduce time and labor, and result in a more representative dataset. The terrestrial laser scanner (TLS) is one of the most widely used instruments in Earth science applications, and it is very useful for acquiring high-quality, high-resolution, three-dimensional (3D) point clouds from outcrops (Xu et al., 2000; Bellian et al., 2005; McCaffrey et al., 2005; Olariu et al., 2008; Jones et al., 2009; Mah et al., 2011; Wilson et al., 2011; Pearce et al., 2011; Mah et al., 2013). In addition, the

GPS receiver module in a typical TLS allows the point cloud, a set of points in a 3D coordinate system, to be transformed into different geographic coordinate systems, so the data can be processed and used for different purposes, such as topographic feature extraction and orientation estimation for planar surfaces.

During the last few years, because of the widespread use of TLS in Earth science applications, there has been a growing need for point cloud processing methods to perform analyses and interpretation. The extraction of fractures and other planar surfaces from 3D outcrop point clouds has been the focus of much research by the geological community because fracture data have a wide range of applications. Many semi-automatic and automatic methods have been developed in the last 10 years, and certain algorithms can be used to extract (or segment) the points of fracture surfaces from the point cloud. [Slob et al. \(2005\)](#) and [Lato et al. \(2009\)](#) derived triangulated irregular networks from the point cloud and then grouped neighboring polygons with a similar orientation to obtain planar features. [Roncella et al. \(2005\)](#), [Voyat et al. \(2006\)](#), and [Ferrero et al. \(2009\)](#) used random sample consensus (RANSAC) algorithm-based methods to segment point clouds into subsets, each of which comprise points that belong to the same discontinuity surface. Recently, other methods have also been proposed based on k-means clustering ([Olariu et al., 2008](#)), moving sampling cube ([Gigli and Casagli, 2011](#)), point attributes ([García-Sellés et al., 2011](#)), neighboring points coplanarity testing ([Riquelme et al., 2014](#)), and principal component analysis (PCA) ([Gomes et al., 2016](#)). However, using these methods, either the full extent of the individual fracture surface is not extracted ([Slob et al., 2005](#); [Olariu](#)

et al., 2008; Lato et al., 2009) or human supervision is required (Ferrero et al., 2009; Gigli and Casagli, 2011; García-Sellés et al., 2011; Riquelme et al., 2014). The automatic method proposed by Gomes et al. (2016) splits the point cloud into four subsets (quadrants) iteratively to detect planar structures, but the full extent of the individual fracture surface was not fully extracted and was detected as several planar structures in most cases.

In this study, we propose an algorithm using a region-growing approach for the automatic extraction of the full extent of individual outcrop fractures from point clouds and for estimating their orientation. The main novel feature of this algorithm is the application of region growing to the extraction of outcrop fractures from point clouds. Instead of growing the region locally without a global view of the fracture surface, we use a seed point selection criterion to consider the overall fracture occurrence, as well as criteria for determining the initial seed point and controlling the growth of the region. The region-growing concept is simple, and by using carefully designed criteria, our algorithm can extract the full extent of every individual fracture in an automatic and robust manner.

2. Study area and database

The study site is a road-cut rock slope located along a country road in Nanbaoxiang, Chengdu, Sichuan Province, China (N $30^{\circ} 24' 25.35''$, E $103^{\circ} 11' 8.34''$) (Fig. 1). The rock slope mainly comprises thin to thick layered sandstone, and the area of the study outcrop is about 30 m^2 . A RIEGL VZ-1000 terrestrial laser scanning system (mainly comprising a 3D laser scanner, digital camera, and GPS receiver) was used to perform a high-resolution

LiDAR scan of the rock slope. This TLS system uses the time-of-flight technique, which utilizes the emission and return time of highly collimated electromagnetic radiation to calculate the distance from the instrument's optical center to a reflecting target surface (Baltsavias, 1999). An outcrop 3D point cloud was acquired with an average point spacing of < 1 cm; there were about 21 million points. To test the proposed region-growing-based algorithm, we selected the central part of the point cloud (delineated by the white rectangle in Fig. 1), where less vegetation and fallen stone were present. Conventional measurements of fracture surface orientations using a handheld compass were also performed on the rock slope to compare with the results obtained by the proposed algorithm, and 65 orientation measurements (dip direction and dip angle) were acquired from fracture faces distributed over the outcrop.



Figure 1: Picture of the study site: a road-cut rock slope with thin to thick layered sandstone. The white rectangle delineates the part used to test our algorithm. See the red notebook for scale.

3. Methodology

Region growing is an element-based segmentation method, which has many advantages compared with other methods. The concept of region growing is simple; only a small number of seed points and a few criteria are required to grow the region. Region growing can correctly segment regions that share the same defined properties. The seed points and the criteria can be selected freely to suit different applications. A drawback of region growing is that it lacks a global view of the problem; however, this drawback can be addressed by selecting criteria that consider the global view of the problem during the region growing, and this we do in our proposed algorithm.

The proposed region-growing-based algorithm works directly with the LiDAR point cloud instead of using an interpolated 2.5D mesh surface. Many detailed geometrical features extracted from the point cloud of the outcrop surface can be used for the segmentation, but the proposed algorithm uses mainly the local surface normal and curvature.

The proposed method comprises three main steps, as follows. First step: Local surface normal and curvature estimation, which involves a nearest-neighbor search as well as the estimation of the least-squares fitting plane and the curvature of the neighboring points. This task is described in Section 3.1. Second step: Region growing, which extracts the fracture face by using criteria based on the local surface normal and curvature to select the seed points and to control the growth. This step is explained in Section 3.2. Third step: Fracture orientation estimation, which employs a patch of the point cloud after its growth is complete. This part is described in Section 3.3.

3.1. Local surface normal and curvature estimation

One or more properties of each point in the point cloud are required for region-growing segmentation, i.e., segmenting the regions that comprise points with similar defined properties. The local surface normal and the local surface curvature are two basic properties that can be used to define planar surfaces such as fractures.

To estimate the local surface normal and curvature for each point, its neighboring points, which together form the local topography, are needed. We refer to a point cloud as P , a collection of 3D points $\mathbf{p}_i = \{x_i, y_i, z_i\} \in P$. Let \mathbf{p}_q be the query point in the problem of estimating the local surface normal and curvature, and let P^k be the k -nearest neighbors of \mathbf{p}_q , in which k is chosen by the user to find the k nearest neighbors according to their Euclidean distance to \mathbf{p}_q .

The method we use for estimating the local surface normal is based on least-squares plane fitting with P^k , as proposed by [Berkmann and Caelli \(1994\)](#). The least-squares plane fitting method is based on PCA. The local surface normal \mathbf{n}_q of point \mathbf{p}_q is obtained by analyzing the eigenvalues and eigenvectors of P^k 's covariance matrix $C = \frac{1}{k} \sum_{i=1}^k (\mathbf{p}_i - \bar{\mathbf{p}}) \cdot (\mathbf{p}_i - \bar{\mathbf{p}})^T$, where $\mathbf{p}_i \in P^k$ and $\bar{\mathbf{p}} = \frac{1}{k} \cdot \sum_{i=1}^k \mathbf{p}_i$. If we let λ_0 , λ_1 , and λ_2 be the eigenvalues of C that satisfy $0 \leq \lambda_0 \leq \lambda_1 \leq \lambda_2$ and if \mathbf{v}_0 is the corresponding eigenvector of λ_0 , then

$$\mathbf{n}_q = \begin{cases} \mathbf{v}_0 & \text{if } \mathbf{v}_0 \cdot (\mathbf{v}_p - \mathbf{p}_q) > 0 \\ -\mathbf{v}_0 & \text{if } \mathbf{v}_0 \cdot (\mathbf{v}_p - \mathbf{p}_q) < 0, \end{cases} \quad (1)$$

where \mathbf{v}_p is the viewpoint from which the point cloud is acquired.

The method used to estimate the local surface curvature was proposed

by Pauly et al. (2002). This method can estimate the curvature directly from the eigenvalues of P^k 's covariance matrix C without needing to first create a surface from the point cloud. The local surface curvature σ_q of \mathbf{p}_q is estimated as follows.

$$\sigma_q = \frac{\lambda_0}{\lambda_0 + \lambda_1 + \lambda_2} \quad (2)$$

3.2. Region growing

Let $P_r \subset P$ be the set of points that have not yet been assigned to any fracture regions. For each fracture region, the initial seed point that starts this region's growth is selected from P_r , and the point $\mathbf{p}_{\min} \in P_r$ with the minimum curvature is selected as a reasonable initial seed point for planar surfaces such as fractures.

Next, the criterion that controls the growth from the seed points to their neighboring points is defined as the local surface normal deviation threshold θ_{th} given by the user. For the neighboring point \mathbf{p}_i , the local surface normal is \mathbf{n}_i , and the seed point's local surface normal is \mathbf{n}_s , so \mathbf{p}_i is added to the current region if $\cos^{-1}\left(\frac{\mathbf{n}_s \cdot \mathbf{n}_i}{\|\mathbf{n}_s\| \|\mathbf{n}_i\|}\right) < \theta_{\text{th}}$, i.e., if the angle between \mathbf{n}_s and \mathbf{n}_i is less than θ_{th} .

The new seed points are then selected from the newly added points. The criterion defined as the transmission error threshold t_{th} , which is also given by the user, determines whether the newly added \mathbf{p}_i is selected as a new seed point. For the newly added \mathbf{p}_i , the local surface normal is \mathbf{n}_i and the initial seed point \mathbf{p}_{\min} 's local surface normal is \mathbf{n}_{\min} , so the newly added \mathbf{p}_i is selected as a new seed point if $\cos^{-1}\left(\frac{\mathbf{n}_{\min} \cdot \mathbf{n}_i}{\|\mathbf{n}_{\min}\| \|\mathbf{n}_i\|}\right) < t_{\text{th}}$, i.e., if the angle between \mathbf{n}_{\min} and \mathbf{n}_i is less than t_{th} . Therefore, the overall occurrence of the

fracture, which is represented by \mathbf{n}_{\min} , serves to control the growth of the region instead of its being allowed to grow blindly.

The region's growth from the newly selected seed points and the selection of new seed points are then performed iteratively until no new seed point can be selected and the region's growth is complete. The growth of the other regions is completed for those remaining in the point cloud until all of the points in the point cloud have been processed.

The local surface normal deviation threshold θ_{th} and the transmission error threshold t_{th} that yield the best segmentation result are related to the fracture surface's geometrical nature and the weathering condition of the outcrop. According to their definitions and the functions described above, θ_{th} is related to the local roughness, whereas t_{th} is related to the overall flatness of the fracture. For example, if a flat fracture has a rough local surface, then θ_{th} should be sufficiently large to allow small protrusions and dents in the fracture region. If the uneven fracture has a smooth local surface, such as weathered fracture surfaces, then t_{th} should be sufficiently large to allow the uneven fracture to grow into one region. The flow chart for the region-growing step of the proposed method is shown in Fig. 2.

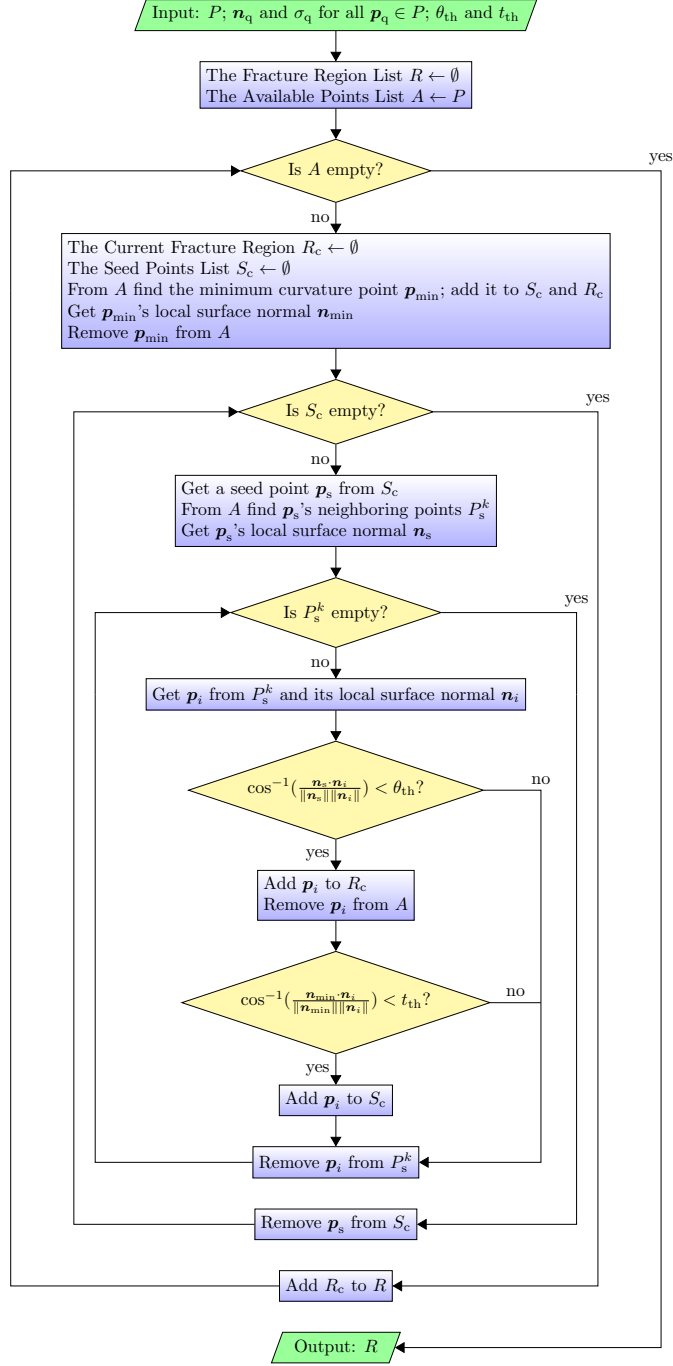


Figure 2: Flowchart illustrating the region-growing algorithm used by the proposed method.

3.3. Fracture orientation estimation

For a patch of a point cloud that has completed its growth, many features of the extracted fracture can be estimated, such as the fracture orientation. The fracture orientation can be estimated as the normal $\langle n_x, n_y, n_z \rangle$ of the least-squares fitting plane in the point cloud patch that represents the fracture. The normal can also be transformed into the $\langle \text{Dip direction}, \text{Dip} \rangle$, and the transformation may vary with the geographic coordinate systems employed for the point cloud. For example, if the y-axis of the coordinate system points north, the x-axis points east, and the z-axis points vertically up, then the Dip direction and Dip will be as follows.

$$\text{Dip direction} = \begin{cases} 0^\circ & \text{if } n_x = 0 \ \& \ n_y \geq 0 \\ 180^\circ & \text{if } n_x = 0 \ \& \ n_y < 0 \\ 90^\circ - \tan^{-1}(n_y/n_x) & \text{if } n_x > 0 \\ 270^\circ - \tan^{-1}(n_y/n_x) & \text{if } n_x < 0 \end{cases} \quad (3)$$

$$\text{Dip} = \begin{cases} 0^\circ & \text{if } n_x^2 + n_y^2 = 0 \\ 90^\circ - \tan^{-1}\left(\frac{|n_z|}{\sqrt{n_x^2 + n_y^2}}\right) & \text{if } n_x^2 + n_y^2 \neq 0 \end{cases} \quad (4)$$

4. Results and discussion

The point cloud used to test our algorithm and the conventional measurements of the fracture surface orientations for the same outcrop were described in Section 2. The application of the proposed algorithm to the entire point cloud will provide a great number of planar regions with various dimensions,

and this makes it difficult to show the detailed results obtained by the proposed algorithm. Therefore, before applying the proposed algorithm to the entire point cloud, we tested the algorithm with a portion of the point cloud, as described in Section 4.1. The results obtained for the entire point cloud and comparisons with manual field survey results are discussed in Section 4.2. The performance of the proposed algorithm in terms of time consumption was tested using a set of outcrop point cloud data, and the number of planes detected from the same point cloud data with different configurations of θ_{th} and t_{th} was also investigated. These are discussed in Section 4.3.

4.1. Details of results for a portion of the point cloud

A portion of the outcrop (Fig. 3a and its point cloud Fig. 3b) was processed using our method. The local surface normal deviation threshold θ_{th} was set to 6° , and the transmission error threshold t_{th} was set to 20° , which were tuned to obtain the best results. These settings for θ_{th} and t_{th} can be applied to similar outcrop conditions. Fig. 3c is the result of the proposed algorithm; it shows the fracture regions having more than 800 points so that they can be conveniently compared with the manually identifiable fractures in Fig. 3a. The threshold value of 800 can be modified if smaller or larger fracture regions are required. Different fracture regions are indicated by different colors; the non-fracture regions are shown in red.

The results show that most of the fractures extracted by the proposed algorithm could be identified as real fractures in Fig. 3a and also that most of the major fractures identified in Fig. 3a were extracted by the proposed algorithm. In addition, the results show that unlike other existing methods, the proposed region-growing-based algorithm can extract the full extent of

every individual fracture automatically.

The estimated fracture planes and the least-squares fitting planes for the extracted fracture regions are shown in Fig. 3d. The fracture orientations were estimated using these planes according to the methods described in Section 3.3.

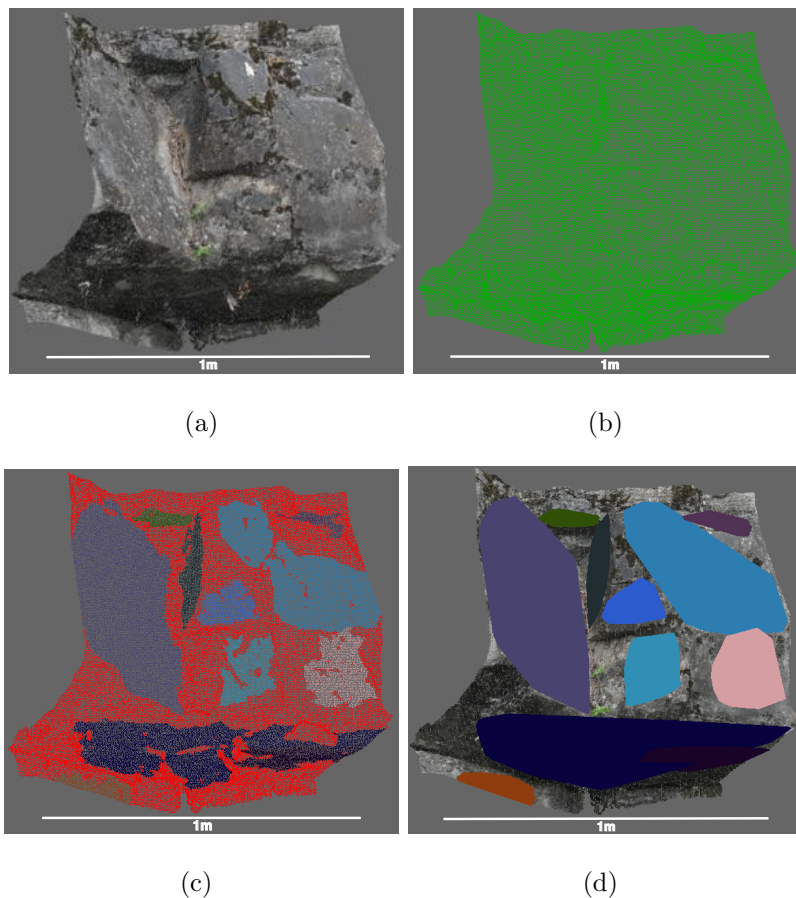


Figure 3: Detailed results obtained from a portion of the point cloud. (a) A portion of the outcrop and (b) its point cloud. (c) Segmentation results obtained using the proposed algorithm. Different fracture regions are shown in various colors, and the non-fracture regions are shown in red. (d) Estimated fracture planes obtained from the segmentation results.

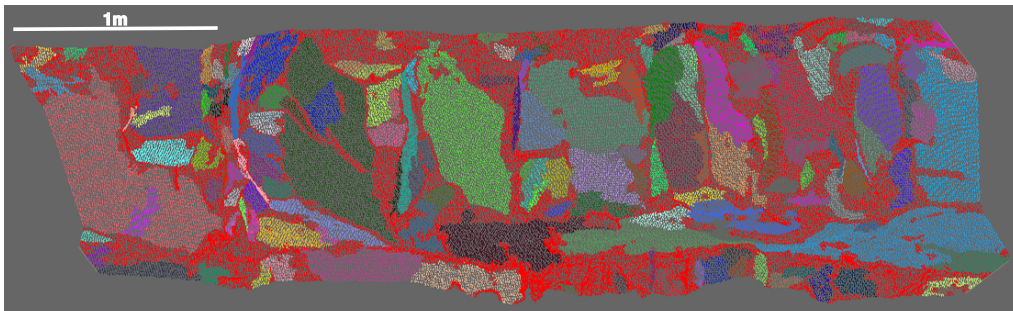
4.2. Results for entire point cloud and comparison with manual field survey results

We applied the proposed method, with the local surface normal deviation threshold θ_{th} set to 6° and the transmission error threshold t_{th} set to 20° , to the entire point cloud (Fig. 4a). The resulting fracture regions having more than 100 points are shown by different colors in Fig. 4b, and the non-fracture regions are shown in red.

The results demonstrate that our proposed algorithm can extract many small fracture faces, cases for which conventional measurements cannot be obtained. Thus, besides accurately extracting fractures in the same manner as a conventional manual survey as demonstrated by the detailed results shown in Section 4.1, our method may also provide additional information about fractures (particularly small fractures) that cannot be acquired from conventional manual surveys.



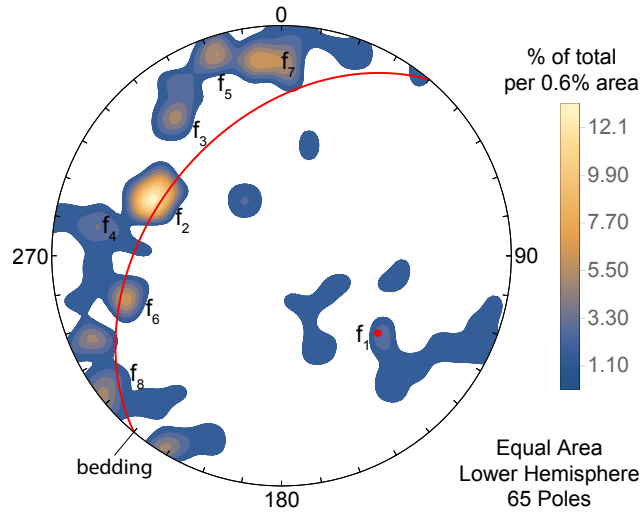
(a)



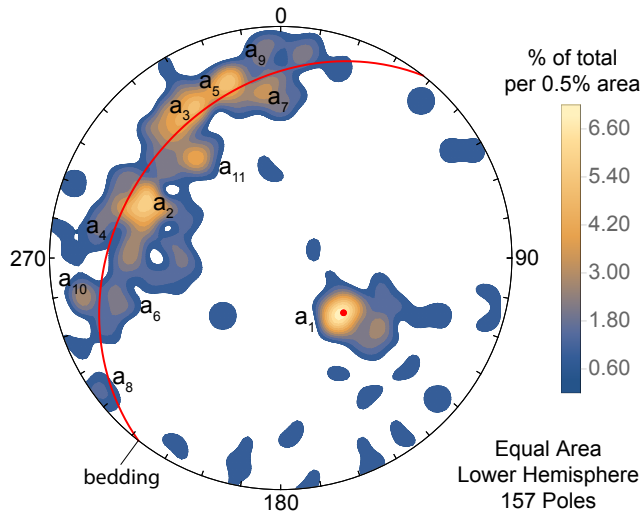
(b)

Figure 4: (a) The outcrop used to test the proposed algorithm and (b) the segmentation results. Different fracture regions are shown by different colors, and the non-fracture regions are shown in red.

We extracted 157 fracture regions having more than 100 points and estimated their orientations. To compare the performance of the manual field survey and our proposed algorithm, we stereographically projected 65 orientations from the manual field survey and 157 orientations from the results obtained by the proposed algorithm and plotted the density of their poles (Fig. 5a and Fig. 5b, respectively).



(a)



(b)

Figure 5: Pole density plots for the fracture orientations obtained from (a) the manual field survey and (b) the results produced using the proposed algorithm. The bedding's pole and arc plot are each shown in red in both (a) and (b). f_1, \dots, f_8 and a_1, \dots, a_8 represent different sets of corresponding fractures.

A comparison of the pole density plots shows that the major clusters of poles representing different sets of fractures from the field manual survey, such as f_1, \dots, f_8 in Fig. 5a, can also be found in the results obtained using our algorithm (a_1, \dots, a_8 in Fig. 5b). The comparison also shows that the proposed algorithm has the advantage of locating clusters of fracture sets more accurately. For example, if many fractures are perpendicular to the bedding (as was found at the study site considered), then the stereographic plot poles of those fractures should be near the arc of the bedding, and obviously the proposed algorithm has better descriptions than the manual field survey. Thus, the red arc of bedding in Fig. 5b fits the distribution of poles better than the red arc of bedding in Fig. 5a, which indicates that our algorithm was better at locating the cluster of bedding and the other clusters of fracture sets. Therefore, in general, our algorithm was able to obtain fracture data whose quality was as good as or better than that from the manual field survey.

Furthermore, our algorithm provides additional information about fractures, which may be useful for the analysis. For example, clusters a_9, a_{10} and a_{11} in Fig. 5b, as well as the symmetries between a_6 and a_7 , a_9 and a_{10} , a_6 and a_{10} , and a_7 and a_9 , may be interesting information that merits further discussion and study.

The only disadvantage of the proposed algorithm may be the presence of some possible outlier clusters in the fracture sets (examples can be seen in Fig. 5b). The nature and removal of these outliers should be studied in future work.

4.3. Performance and parameter configuration of the proposed algorithm

A set of point cloud data (Table 1) was used to test the performance of our algorithm using a desktop computer with a CPU of 3.60 GHz and 4 GB RAM. The average point spacing in all the point cloud datasets used was 0.01 m, the dataset size ranged from 134,067 points to 1,096,948 points, and the outcrop areas ranged from 5.5 m² to 67.3 m². The same processing parameters were used for all the point cloud datasets to highlight the variation in the time consumption.

Table 1: Point cloud datasets used to test the performance of the proposed region-growing-based algorithm

Dataset	Number of points	Average point spacing (m)	Area (m ²)
1	134,067	0.01	5.5
2	323,562	0.01	14.5
3	484,658	0.01	19.0
4	684,866	0.01	33.7
5	1,096,948	0.01	67.3

The performance testing result is shown in Fig. 6. The figure shows that there was a step increase in time consumption as the point cloud size reached 1 million points, but the time consumption is still acceptable. Therefore, we conclude that our algorithm is suitable for point cloud datasets whose outcrop area ≤ 70 m². For datasets larger than that, the computing power should be increased or the algorithm should be modified.

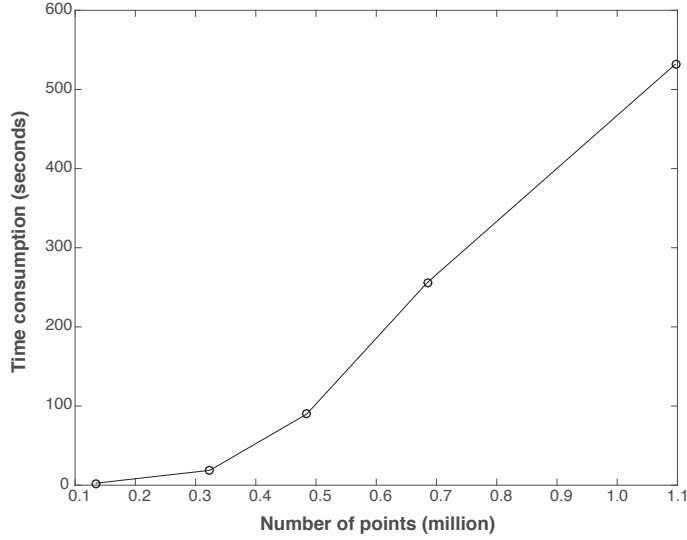
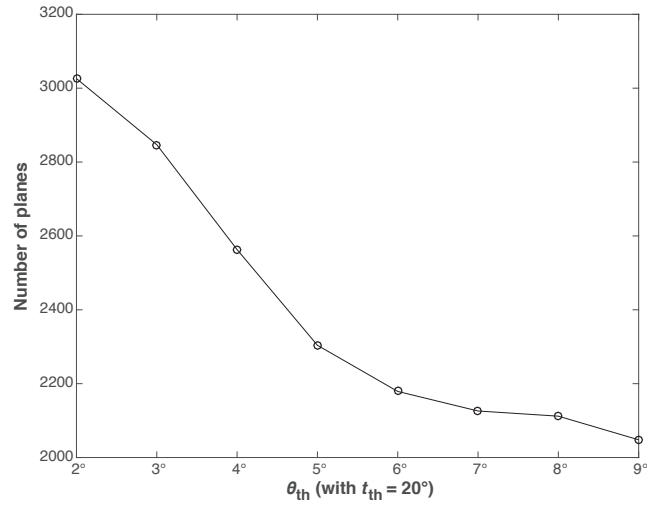


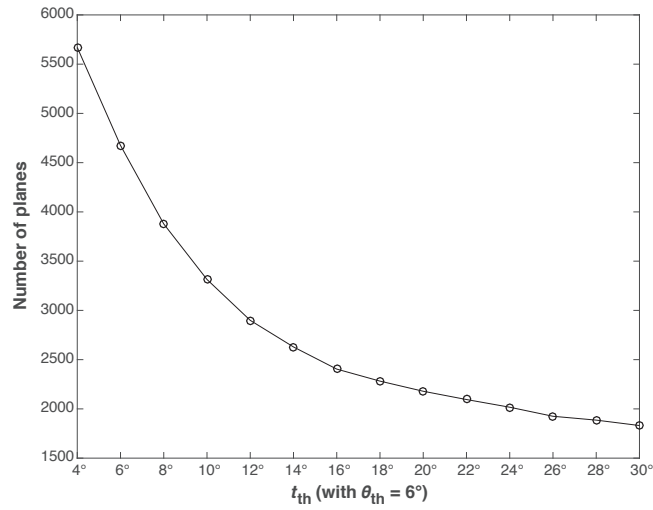
Figure 6: Time consumption of the proposed region-growing-based algorithm as point cloud size (number of points) increases.

Using the same point cloud as the one shown in Fig. 4a, we investigated the number of planes detected using different configurations of θ_{th} and t_{th} . The results are shown in Fig. 7, which shows that an increase in θ_{th} or t_{th} resulted in a decrease in the number of planes detected. It is interesting to note that $\theta_{th} = 6^\circ$ in Fig. 7a and $t_{th} = 20^\circ$ in Fig. 7b, the configuration we judged to yield the best results, are turning points: before these points, the number of planes detected decreases quickly; after these points, the number of planes detected decreases much more slowly. As we know, small changes in the configuration of θ_{th} and t_{th} should not greatly influence the number of planes detected, so the point cloud may be over-segmented before these turning points. Thus, an analysis of the number of planes detected under different configurations of θ_{th} and t_{th} may help find the configuration that

yields the best results.



(a)



(b)

Figure 7: Number of planes detected from the same point cloud under different configurations of (a) θ_{th} and (b) t_{th} .

5. Conclusion

In this paper, we have proposed an innovative region-growing-based method for automatically extracting outcrop fractures from 3D point clouds. Two local topographic features of the point cloud, i.e., the local surface normal and curvature, are used to define planar surfaces such as fractures. By their definitions, the local surface normal deviation threshold θ_{th} and the transmission error threshold t_{th} are designed to control the growth of the fracture regions; t_{th} considers the overall occurrence of the fracture while controlling the region growth so that it is not allowed to grow blindly. The orientations are estimated for each extracted fracture.

We tested the proposed method using a 3D point cloud acquired for a real outcrop at the study site, and the results obtained were compared with data collected by a manual field survey for the same outcrop. The test results showed that unlike the existing automatic or semi-automatic methods, the new algorithm can extract the full extent of every individual fracture automatically and accurately. The comparison between our method and the manual field survey shows that the proposed region-growing-based algorithm can obtain fracture data whose quality is as good as or better than that of the manual field survey, thereby demonstrating the potential utility of our method. The performance test using a set of point cloud data showed that the proposed algorithm is suitable for point cloud datasets whose outcrop area ≤ 70 m². The analysis of the number of planes detected under different configurations of θ_{th} and t_{th} helped explain the configuration we had judged to yield the best results; such analysis may provide a way to find the configuration that yields the best results.

Further research should focus on improving the proposed method by removing possible non-fracture regions (outlier clusters in the fracture sets) and analyzing the results obtained by the region-growing-based algorithm, such as the relationship between the roughness of the fracture and the weathering condition, fracture type, and orientation, as well as assessing the performance of the proposed method with different rock types and weathering conditions.

Acknowledgments

This study was funded by the Chinese National Science and Technology Major Project (2011ZX05009001). We are grateful to Prof. Changjiang Li for valuable comments on earlier drafts. We would like to thank the editor and two anonymous reviewers for their valuable comments and suggestions, which have improved the paper.

References

- Baltsavias, E.P., 1999. Airborne laser scanning: basic relations and formulas. *ISPRS Journal of Photogrammetry and Remote Sensing* 54, 199–214.
- Bellian, J.A., Kerans, C., Jennette, D.C., 2005. Digital Outcrop Models: Applications of Terrestrial Scanning Lidar Technology in Stratigraphic Modeling. *Journal of Sedimentary Research* 75, 166–176.
- Berkmann, J., Caelli, T., 1994. Computation of surface geometry and segmentation using covariance techniques. *IEEE Transactions on Pattern Analysis and Machine Intelligence* 16, 1114–1116.

- Ferrero, A.M., Forlani, G., Roncella, R., Voyat, H.I., 2009. Advanced Geostructural Survey Methods Applied to Rock Mass Characterization. *Rock Mechanics and Rock Engineering* 42, 631–665.
- García-Sellés, D., Falivene, O., Arbués, P., Gratacos, O., Tavani, S., Muñoz, J.A., 2011. Supervised identification and reconstruction of near-planar geological surfaces from terrestrial laser scanning. *Computers & Geosciences* 37, 1584–1594.
- Gigli, G., Casagli, N., 2011. Semi-automatic extraction of rock mass structural data from high resolution LIDAR point clouds. *International Journal of Rock Mechanics and Mining Sciences* 48, 187–198.
- Gomes, R.K., de Oliveira, L.P., Gonzaga, L., Tognoli, F.M., Veronez, M.R., de Souza, M.K., 2016. An algorithm for automatic detection and orientation estimation of planar structures in LiDAR-scanned outcrops. *Computers & Geosciences* 90, 170–178.
- Jones, R.R., Kokkalas, S., McCaffrey, K.J.W., 2009. Quantitative analysis and visualization of nonplanar fault surfaces using terrestrial laser scanning (LIDAR)—The Arkitsa fault, Central Greece, as a case study. *Geosphere* 5, 465–482.
- Lato, M., Diederichs, M.S., Hutchinson, D.J., Harrap, R., 2009. Optimization of LiDAR scanning and processing for automated structural evaluation of discontinuities in rockmasses. *International Journal of Rock Mechanics and Mining Sciences* 46, 194–199.

- Mah, J., Samson, C., McKinnon, S.D., 2011. 3D laser imaging for joint orientation analysis. *International Journal of Rock Mechanics and Mining Sciences* 48, 932–941.
- Mah, J., Samson, C., McKinnon, S.D., Thibodeau, D., 2013. 3D laser imaging for surface roughness analysis. *International Journal of Rock Mechanics and Mining Sciences* 58, 111–117.
- McCaffrey, K., Jones, R., Holdsworth, R., Wilson, R., Clegg, P., Imber, J., Holliman, N., Trinks, I., 2005. Unlocking the spatial dimension: digital technologies and the future of geoscience fieldwork. *Journal of the Geological Society* 162, 927–938.
- Olariu, M.I., Ferguson, J.F., Aiken, C.L., Xu, X., 2008. Outcrop fracture characterization using terrestrial laser scanners: Deep-water Jackfork sandstone at Big Rock Quarry, Arkansas. *Geosphere* 4, 247–259.
- Pauly, M., Gross, M., Kobbelt, L.P., 2002. Efficient simplification of point-sampled surfaces, in: *Proceedings of the conference on Visualization'02*, IEEE Computer Society. pp. 163–170.
- Pearce, M.A., Jones, R.R., Smith, S.A., McCaffrey, K.J., 2011. Quantification of fold curvature and fracturing using terrestrial laser scanning. *AAPG Bulletin* 95, 771–794.
- Riquelme, A.J., Abellán, A., Tomás, R., Jaboyedoff, M., 2014. A new approach for semi-automatic rock mass joints recognition from 3D point clouds. *Computers & Geosciences* 68, 38–52.

- Roncella, R., Forlani, G., Remondino, F., 2005. Photogrammetry for geological applications: automatic retrieval of discontinuity orientation in rock slopes, in: *Electronic Imaging 2005*, International Society for Optics and Photonics. pp. 17–27.
- Slob, S., van Knapen, B., Hack, R., Turner, K., Kemeny, J., 2005. Method for Automated Discontinuity Analysis of Rock Slopes with Three-Dimensional Laser Scanning. *Transportation Research Record: Journal of the Transportation Research Board* , 187–194.
- Voyat, I., Roncella, R., Forlani, G., Ferrero, A.M., et al., 2006. Advanced techniques for geo structural surveys in modelling fractured rock masses: application to two Alpine sites, in: *Golden Rocks 2006*, The 41st US Symposium on Rock Mechanics (USRMS), American Rock Mechanics Association.
- Wilson, C.E., Aydin, A., Karimi-Fard, M., Durlofsky, L.J., Sagy, A., Brodsky, E.E., Kreylos, O., Kellogg, L.H., 2011. From outcrop to flow simulation: Constructing discrete fracture models from a LIDAR survey. *AAPG Bulletin* 95, 1883–1905.
- Xu, X., Aiken, C.L.V., Bhattacharya, J.P., Corbeanu, R.M., Nielsen, K.C., McMechan, G.A., Abdelsalam, M.G., 2000. Creating virtual 3-D outcrop. *The Leading Edge* 19, 197–202.